Appl Microbiol Biotechnol
DOI 10.1007/s00253-013-5121-5

Quantitative monitoring of 2-oxoglutarate in *Escherichia coli* cells by a fluorescence resonance energy transfer-based biosensor

Chang Zhang · Zi-Han Wei · Bang-Ce Ye

Received: 24 April 2013 / Revised: 7 June 2013 / Accepted: 10 July 2013

Abstract 2-Oxoglutarate (2OG) is a metabolite from the highly conserved Krebs cycle and not only plays a critical role in metabolism but also acts as a signaling molecule in a variety of organisms. Environmental inorganic nitrogen is reduced to ammonium by microorganisms, whose metabolic pathways involve the conversion of 2OG to glutamate and glutamine. Tracking of 2OG in real time would be useful for studies on cell metabolism and signal transduction. Here, we developed a genetically encoded 2OG biosensor based on fluorescent resonance energy transfer by inserting the functional 2OG-binding domain GAF of the NifA protein between the fluorescence resonance energy transfer (FRET) pair YFP/CFP. The dynamic range of the sensors is 100 μM to 10 mM, which appeared identical to the physiological range observed in *E. coli*. We optimized the peptide lengths of the binding domain to obtain a sensor with a maximal ratio change of 0.95 upon 2OG binding and demonstrated the feasibility of this sensor for the visualization of metabolites both in vitro and in vivo.

Keywords Genetically encoded biosensor · Fluorescent protein · FRET · 2-Oxoglutarate · In vivo imaging

Introduction

2-Oxoglutarate (2OG) is derived from the Krebs cycle (Zhao et al. 2010), which is a highly conserved central metabolic pathway, and is at the interface between carbon and nitrogen metabolism. The central carbon intermediate 2OG also serves as the sole carbon skeleton for the assimilation of nitrogen, and it participates in the generation of glutamate through the glutamine synthetase/glutamate synthase (GS/GOGAT) system. GS assimilates ammonia by converting glutamate to glutamine. GOGAT then transfers the amido group of glutamine to 2OG to form two glutamates. Other nitrogen-containing compounds derive nitrogen from glutamate and glutamine by secondary amino transfers. In a wide range of Bacteria and Archaea, 2OG, which is the donor for ammonia assimilation, signals nitrogen deficiency, whereas glutamine, which is the fully aminated product, often signals nitrogen sufficiency. From this perspective, in addition to its importance as a metabolite, 2OG also transmits critical signals in metabolic activities (Martinez-Argudo et al. 2005). In the cytosol of living cells, the signal transduction proteins GlnB and GlnK, which belong to the PII superfamily (Leigh and Dodsworth 2007), sense cellular 2OG or glutamine as an indicator of the nitrogen state. High levels of cellular 2OG, an indicator of nitrogen deficiency, inhibit the GlnB signal system. The physiological 2OG concentrations in *Escherichia coli* have been estimated to be in the 0.1–0.9 mM range under nitrogen-sufficient conditions (Senior 1975). The conventional 2OG quantification method requires the use of cell extracts and is thus incompatible with studying dynamics in intact individual cells; furthermore, it can only provide the averaged 2OG pool concentration of many cells.

Recently, there have been efforts to directly measure and visualize metabolites in cell by using genetically encoded fluorescence resonance energy transfer (FRET)-based biosensors, which can be targeted to subcellular compartments to specifically analyze concentration changes within a specific compartment of an intact live cell (Fehr et al. 2005). A series of genetically encoded nanosensors has been constructed that utilizes FRET technology for noninvasive and temporally and spatially resolved monitoring of signal molecules in vivo. The genetically encoded FRET biosensors consist of a recognition

C. Zhang · Z.-H. Wei · B.-C. Ye (✉)
Laboratory of Biosystems and Microanalysis, State Key Laboratory of Bioreactor Engineering, East China University of Science and Technology, Shanghai 200237, China
e-mail: bcye@ecust.edu.cn

Published online: 28 July 2013

module that specifically binds a ligand and is sandwiched between two variants of green fluorescent protein (GFP) (typically CFP and YFP) (Ewald et al. 2011). The efficiency of fluorescence energy transfer between two fluorophores is highly dependent on their distance and orientation (Jares-Erijman and Jovin 2006; Piston and Kremers 2007). Conformational changes caused by ligand binding to this recognition module induce changes in FRET efficiency between the donor and acceptor pair because of the alteration in distance between the fluorophores. With this strategy, fluorescent biosensors have been engineered using many types of protein modules (e.g., enzymes, membrane receptors, and ligand-binding proteins) as substrate-recognition modules to image signaling molecules in living cells, such as glutamate (Hires et al. 2008; Okumoto et al. 2005), hydrogen peroxide (Yano et al. 2010), cAMP (DiPilato et al. 2004; Ponsioen et al. 2004), ATP (Imamura et al. 2009), cGMP (Honda et al. 2001; Nikolaev et al. 2006), phosphoinositides (Cicchetti et al. 2004), inositol 1,4,5-triphosphate (IP3) (Tanimura et al. 2009), diacylglycerol (Sato et al. 2006), and bacterial quorum-sensing signaling molecules (Rajamani et al. 2007). Recently, various bacterial periplasmic binding proteins (PBPs) from gram-negative bacteria, which undergo a conformational change upon ligand binding, have successfully been used to develop FRET nanosensors for central metabolites such as glutamate, maltose, ribose, arabinose, sucrose, galactose, and glucose (Fehr et al. 2002, 2003; Knetsch et al. 2002; Lager et al. 2003; John et al. 2008).

In this study, we constructed a genetically encoded fluorescent biosensor for 2OG, employing the 2OG-binding domain GAF of the NifA protein derived from the aerobic soil-dwelling organism *Azotobacter vinelandii*. The 2OG-sensing protein NifA belongs to a family of enhancer-binding proteins (EBPs) that activates transcription by RNA polymerase containing the sigma factor (Martinez-Argudo et al. 2004). NifA is a multidomain protein consisting of an amino terminus GAF domain, which is a ubiquitous signaling motif found in signaling, and sensory proteins from all three kingdoms of life (Aravind and Ponting 1997; Ho et al. 2000), a central catalytic (AAA+) domain required to couple nucleotide hydrolysis to activation of the σ^{54}-RNA polymerase holoenzyme, and a carboxyl-terminal DNA-binding domain (Buck et al. 2000; Morett and Segovia 1993). Upon the binding of 2OG to the amino-terminal GAF domain, NifA induces a conformational change and inhibits the binding of NifL to NifA. Mutations conferring resistance to NifL are located in both the GAF and the AAA + domains of NifA. Because it is unclear whether the AAA + domain is necessary for the conformation change, we chose two different parts of NifA, the GAF domain and GAF-AAA + domain, as detector domains to create FRET-based biosensors. The two sensors both exhibited ratio changes on binding to 2OG in vitro, which led to the conclusion that ATPase (AAA + domain) is not vital for the conformational change in the GAF domain. In the presence of ligands, the biosensors showed a concentration-dependent decrease in FRET efficiency. We also systematically engineered the linker moiety by inserting peptide connectors with different lengths. The resulting biosensor with an optimized linker was used to monitor the dynamic in vivo responses of *E. coli* to the addition of different carbon sources and to image 2OG in intact individual cells by using a confocal microscope. This reporter, OGsor, shows the cellular 2OG dynamics in *E. coli* cells upon metabolic challenges.

Materials and methods

Construction of plasmids

The restriction sites for four enzymes — *Bam*HI, *Eco*RI, *Sac*I and *Sal*I — in the pET-28a (+) vector were chosen for tandem fusion of YFP, the 2OG-binding domain (GAF or GAF-AAA+), and CFP to construct a FRET biosensor. CFP and YFP (mutants of EGFP,GenBank Accession #U55762.1) were cloned from the commercially available plasmids pECFP-N1 (Clontech catalog #6900-1) and pEYFP-N1 (Clontech catalog #6006-1). A candidate gene encoding the 2OG reaction domains GAF and GAF-AAA + included in the NifA-encoding gene (*NC_012560.1*) was amplified from the genome of *A. vinelandii* (strain number 10088) purchased from the Agricultural Culture Collection of China (ACCC), Beijing, by polymerase chain reaction (PCR) amplification (TakaRa, Japan). The restriction endonucleases were obtained from New England Biolabs (Ipswich, MA, USA). All the chemicals, including 2OG, L-glutamic acid, and L-glutamine, were of analytical grade and were purchased from Amresco (Solon, OH, USA). *E. coli* DH5α was used as the cloning host and *E. coli* BL21 (DE3)pLysS was used as the protein production host, and they were purchased from TransGen Biotech (Beijing, China).

In vitro assays

E. coli BL21 (DE3) pLysS expressing OGsor was grown for 3 h in LB medium at 37 °C before induction by the addition of 0.5 mM isopropyl-β-D-thiogalactopyranoside (IPTG) overnight. The cell pellet was suspended in 50 mM PBS (pH=8.0) buffer before sonication, and all the analytes were dissolved in the same buffer and adjusted to a final pH of 8.0. Fluorescence was measured in a fluorescence microplate reader (Bio-Tek Instrument, Winooski, VT, USA) by using a black 96-well microplate (Fluotrac 200, Greiner, Germany). Emission wavelengths of 478 and 528 nm, or a continuous spectrum from 460 to 600 nm, were monitored using excitation at 440 nm. The blank measurement was obtained from a well containing only OGsor with a control buffer. FRET levels

have been represented as the ratio of the emission intensities at 528 and at 478 nm when the sensors were excited at 440 nm. The signal intensity with 2OG was defined as the change in the 528/478 ratio. The dissociation constants (K_d) were determined by fitting the titration curves to a single-site-binding isotherm: $R=R_{apo}+(R_{sat}-R_{apo}) \times X/(K_d+X)$ (Ewald et al. 2011), where X is the ligand concentration, R denotes ratio, R_{apo} is the ratio in the absence of ligand, and R_{sat} is the ratio at saturation with ligand. All ratio values were derived from the averages of at least three titration experiments.

2OG pool measurements

For 2OG measurement, 1 ml of cells was collected and immediately washed with 1 ml of the medium. After the tube was centrifuged, it was placed into liquid nitrogen immediately to terminate in vivo metabolism and was then placed in water maintained at room temperature. This early-stage protocol should be performed as quickly as possible to decrease 2OG consumption. The shift between liquid nitrogen and room-temperature water was repeated three times to kill the cells. Before sonication, the cells were suspended in 5 ml of 50 % methanol. The pool value in nanomoles per milliliter of cells at 1.0 OD_{600} was converted directly into a millimolar internal concentration (Okano et al. 2010). 2OG was measured using a Shimadzu Prominence HPLC system (LC-20AT and SPD-20A UV/vis fluorescence detector), where 20 μl of the sample was injected into the HPLC column, which was a C18 reversed-phase main column (ODS-4, 5 μm, 4.0×250 mm), and maintained at 30 °C during separation. The elution buffer was 20 mM K^+ phosphate buffer (pH 7.0). The flow rate was 0.4 ml/min and the detector was set at 233 nm.

In vivo assays

E. coli BL21 (DE3) pLysS expressing OGsor was grown for 3 h in LB medium at 37 °C before induction by the addition of 0.5 mM IPTG overnight. Cultures were stored overnight at 4 °C for sufficient maturation of fluorescence protein, and the fluorescence was measured in a fluorescence microplate reader (Bio-Tek Instrument) using black 96-well microplates (Fluotrac 200; Greiner, Germany). Emission wavelengths of 478 and 528 nm, or a continuous spectrum from 460 to 600 nm, were monitored with excitation at 440 nm. The cells were then starved in carbon-free M9 medium containing 50 mg/l kanamycin sulfate (Kaper et al. 2008) for 4 h at 37 °C, and 190-μl cultures were transferred to 96-well plates. Subsequently, 10 μl of glucose, 2OG, citrate (all final concentrations of 10 mM), or carbon-free M9 was added manually to the cultures. The ratio change before and after the addition of the compounds was determined using a fluorescence microplate reader and shaking at 170 rpm between readings. The fluorescence emission at 478 and 528 nm (excitation wavelength, 440 nm; bandwidth, 2 nm) was recorded.

Live cell imaging

E. coli BL21 (DE3) pLysS expressing OGsor was prepared as mentioned in the "In vivo assays" section. Before live cell imaging, *E. coli* cells were transferred to a cover slide and immobilized in 2 % alginate and Ca^{2+} in a total volume of 10 μl (Fehr et al. 2002). Carbon sources (all final concentrations, 10 mM) were added (volume, 1 μl) on top of the alginate-embedded cells. Images were acquired using a Zeiss 710 laser scanning confocal microscopy (LSCM) system on a Zeiss Axio Observer Z1 inverted microscope with a Plan-Apochromat 63×1.4 NA oil immersion objective. The dual emission intensity ratio was recorded with 458 nm excitation and two emission filters (480 nm/40 for CFP and 535 nm/30 for YFP). Pseudocolor images indicate the change in the YFP/CFP ratio after addition of the carbon source. Considering that exposure of a single cell to high laser power would lead to photobleaching, a field containing approximately 50 *E. coli* cells was chosen for laser excitation, but even under this condition, photobleaching occurred after detection for 10 min.

Results

Design and characterization of FRET-based biosensors

To develop a FRET sensor for in vivo real-time monitoring of 2OG, we screened many 2OG-binding domains and finally focused on the GAF domain for its specific binding of 2OG and conformational changes and found that the monomer form is suitable for FRET sensor construction. We excluded GlnB, GlnK (homotrimer), and NifI1/NifI2 (heterohexamer) from the PII superfamily because polymerization may affect FRET efficiency. The intact GAF domain of NifA from *A. vinelandii* was used as the binding domain, and it was sandwiched directly with enhanced cyan FP (CFP) and yellow FP (YFP). NifA contains three domains: an N-terminal GAF domain, a catalytic (AAA+) domain, and a C-terminal DNA-binding HTH domain (Fig. 1a). It is known that 2OG binding of the GAF domain can be allosterically transduced into a conformational change in NifA. Conformational change in the GAF domain is likely to lead to a change in FRET efficiency between CFP and YFP in the sandwich configuration described above. Two FRET-based biosensors were generated by flanking the GAF domain (for OGsor-G) and GAF-AAA + domain (for OGsor-GA) with CFP and YFP to investigate the FRET efficiency responding to 2OG (Fig. 1b,c). The tandem fused proteins were expressed in *E. coli* BL21 (DE3) pLysS (Chen et al. 2004). Two OGsors were excited at 440 nm, and their emission spectra showed two peaks corresponding to

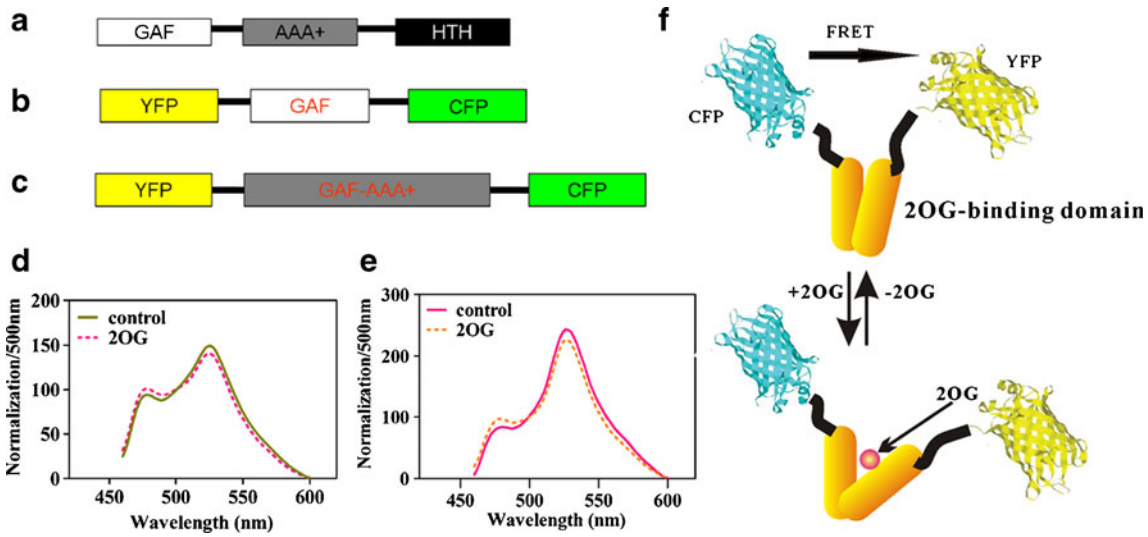

Fig. 1 Schematic representation of NifA (**a**), OGsor-G (**b**), and OGsor-GA (**c**). Fluorescence emission spectra of OGsor-G (**d**) with (*dotted line*) and without (*solid line*) 1 mM (final concentration) 2OG. The FRET sensor OGsor-G was analyzed, and the fluorescence emission was recorded using an excitation wavelength of 440 nm in a fluorescence plate reader. The FRET sensor OGsor-GA (**e**) was detected in the same manner. **f** Energy transfer illustration: 2OG binding caused a conformational change that decreased the energy transferred from CFP to YFP

CFP and YFP. Addition of 2OG resulted in an increase in CFP emission and a decrease in YFP emission. The ratio between the YFP and CFP emission intensities of the two OGsors changed upon addition of 2OG, which demonstrates that the conformation change in the 2OG-recognition domain GAF is translated into a change in FRET efficiency (Fig. 1d,e). The decrease in the 528/478 ratio induced by 2OG suggests that 2OG binding may transform GAF domain into an open conformation from a relatively closed form, thereby resulting in low FRET efficiency (Fig. 1f).

Fluorescence analyses of OGsor-G and OGsor-GA showed that the 528/478 ratios without 2OG were 1.38 and 2.32, respectively. When the 2OG concentration was changed from 10 μM to 10 mM, the emission ratios for the OGsors decreased, following sigmoid curves (Fig. 2a and Table 1), and the maximum changes in the ratios were calculated as −0.16 and −0.42, respectively. OGsor-GA exhibited a ratio change of 18 % (in % R_{apo}), which represents an improvement of approximately 50 % over the 12 % ratio change observed for OGsor-G. The 528/478 ratio changed upon addition of 2OG in a concentration-dependent and saturable manner. The dynamic response range of the OGsor sensors was 100 μM–10 mM. The dissociation constant (K_d) values of OGsor-G and OGsor-GA for 2OG were found to be 687.4 and 635.8 μM, respectively (Table 1). The dynamic ranges of the OGsors corresponded to the physiological range observed in *E. coli*, which varies from 100 μM under conditions of nitrogen excess to 1 mM under conditions of nitrogen limitation.

To test the specificity of the OGsors for 2OG, a panel of related metabolite compounds consisting of citrate, isocitrate, glutamate, and glutamine was applied to the OGsor sensors. OGsor-G and OGsor-GA were both highly selective for 2OG and did not exhibit apparent ratio changes in the presence of other metabolites (Fig. 2b,c) present at their physiological concentrations in *E. coli* (Bennett et al. 2009).

Optimization for the improved 2OG sensor

The response magnitude and dynamic range of the FRET signal can be efficiently increased by inserting peptide linkers between the fluorescent protein and binding domain (Ha et al. 2007). In this study, peptide linkers were genetically fused to FRET-based 2OG sensors to improve the response. A set of OGsors with varying numbers of linker units (Gly4Ser) was tested. No obvious improvement was observed, which implies that the short linker moiety had a negligible effect on the FRET efficiency of OGsors because these linkers did not sufficiently change the distance or fluorophore dipole orientation between YFP and CFP. Another approach for optimization is to change the fluorophore dipole orientation (Ansbacher et al. 2012; Iqbal et al. 2008) which would change the energy transfer efficiency. A previous study took a more rigorous approach that used a circularly permuted GFP (cpGFP) to vary the relative orientation of the transition dipoles of the two chromophores and thereby achieve an obvious optimization effect (Nagai et al. 2004). Compared with OGsor-G (Table 1), OGsor-GA exhibited a better ratio change (50 % increase in % R_{apo}), which could be considered as a type of linker moiety optimization. Thus, the improvement in OGsor-GA may have resulted from the 2-domain configuration of the ATPase AAA + domain (201 amino acids) attached to the GAF domain. To further maximize the

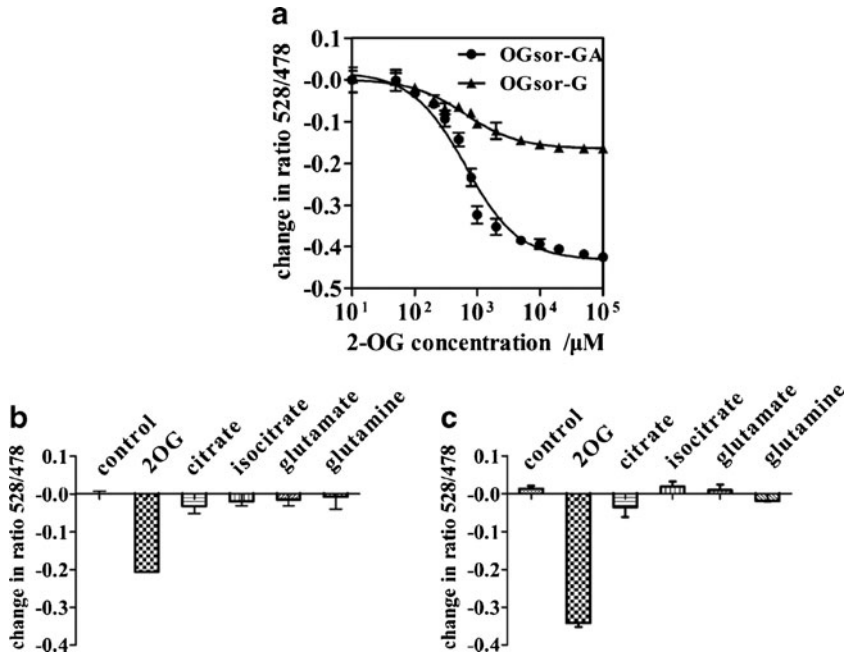

Fig. 2 **a** Binding curve of 2OG with the FRET nanosensors OGsor-G and OGsor-GA. The emission ratio of 528/478 nm was determined at different 2OG concentrations. Data were fitted to a single site-binding curve (*black line*) as described in the "Materials and methods" section. The substrate specificity of the two FRET sensors was compared. The ratio change for OGsor-G (**b**) and OGsor-GA (**c**) was tested in the presence of various elements at physiological concentration levels in *E. coli*, i.e., 2OG (1 mM), citrate (1 mM), isocitrate (1 mM), glutamate (100 mM), and glutamine (10 mM). Data were analyzed in triplicate, and error bars indicate standard deviations

response magnitude of OGsor, we chose the AAA + domain as a displacement target based on the GAF-AAA + domain to obtain a series of 2OG sensors (Fig. 3a and Table 2), with a 20-amino-acid sequence used as a longer linker unit at the C terminal. This displacement approach has great potential to change both the distance and orientation between fluorophores. Among these OGsors, OGsor-G3 yielded an increase in the 528/478 ratio, which indicates that OGsor-G3 formed a structure upon binding of 2OG that brought the two fluorophores closer or that the energy transfer efficiency was enhanced. OGsor-G5 showed no response to 2OG, possibly because of a rigid structure, whereas OGsor-G9 attained the highest ratio change, i.e., a 258 % Δratio increase (in % R_{apo}) relative to OGsor-G (Fig. 3d).

Molecular imaging and analysis of 2OG in *E. coli* cells

FRET sensors allow the collection of real-time data to study the kinetics of metabolite accumulation. In this study, we also tested the ability of the OGsor to detect intracellular 2OG levels in living *E. coli* cells in vivo under different culture conditions. 2OG is a key intermediate in central metabolism and is located at the interface between the Krebs cycle and the assimilatory pathway of nitrogen. The effect of carbon on cellular 2OG levels was investigated first using a medium-shift scheme. *E. coli* BL21 (DE3) pLysS cells expressing OGsor-G9 in LB medium were transferred to carbon-free M9 medium. The emission spectra of cells in LB and M9 media are shown in Fig. 4a. The carbon-free culture resulted in an increase in the emission ratio from 1.67 to 2.27, which indicates a drop in the intracellular 2OG level and quick depletion of 2OG upon removal of carbon. Glucose, as a favored carbon source, can be converted to 2OG through the glycolysis pathway and Krebs cycle. We next monitored the dynamics of 2OG levels in *E. coli* cells after the addition of exogenous citrate and glucose. Citrate was used as the control for the ratio monitoring experiments, as *E. coli* cells do not metabolize citrate as a carbon source under aerobic conditions (Pos et al. 1998). Figures 2 and 4b show that citrate and glucose had no effect on the YFP/CFP emission ratio of the 2OG-specific FRET sensor OGsor. Citrate and glucose were added at concentrations of up to 10 mM to the *E. coli* cells in M9 medium. Figure 4c shows the time-dependent change in the emission ratio following the addition of carbon compounds. The addition of glucose induced an increase in CFP intensity and a decrease in YFP intensity, which rapidly decreased the YFP/CFP emission ratio (i.e., an increase in the 2OG level was indicated). As expected, glucose was immediately internalized and metabolized through glycolysis, which then activated the Krebs cycle. These results suggest that the 2OG pool was subjected to quick accumulation in response to glucose availability. Interestingly, the intracellular 2OG level reached an apparent peak at 30 min after the addition of glucose and then slowly decreased. The slow decrease in the 2OG level was likely the result of exhaustion of glucose and a cellular response to increased cellular 2OG. In contrast to the

Table 1 Characterization of the biosensors OGsor-G and OGsor-GA

Sensor	K_d (μM)	R_{apo}	R_{sat}	Ratio change (% R_{apo})
OGsor-G	687.4	1.38	1.22	−0.16 (12 %)
OGsor-GA	635.8	2.32	1.90	−0.42 (18 %)

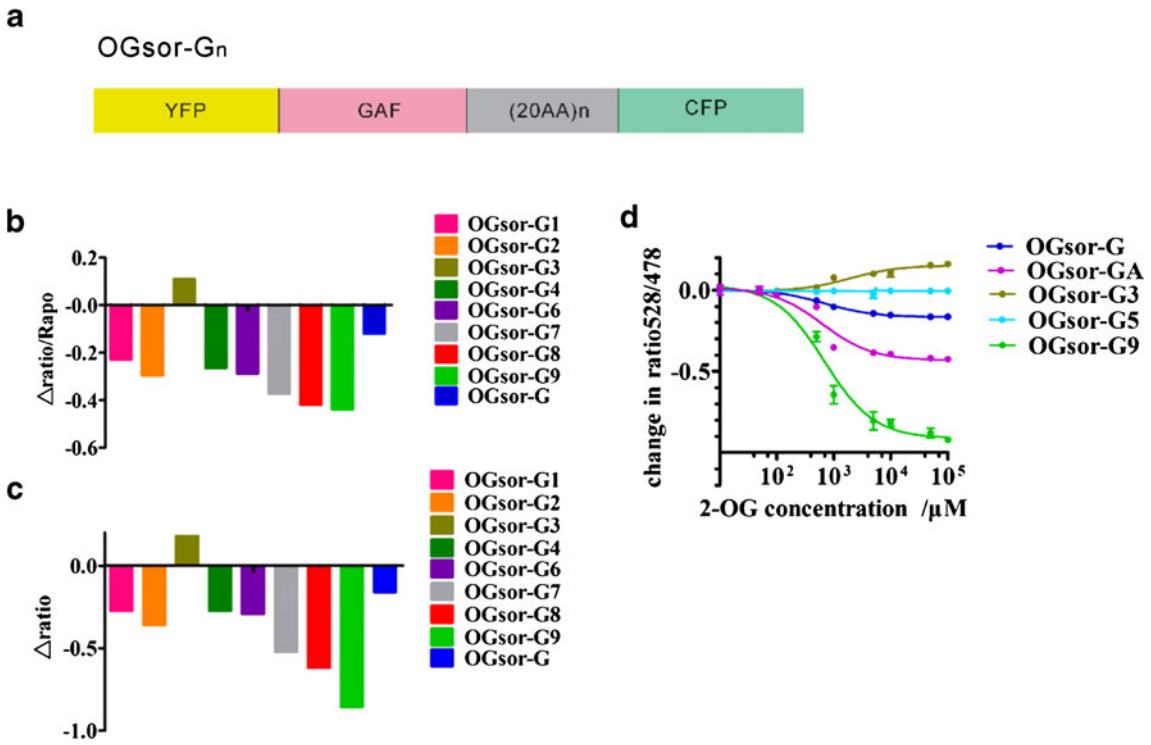

Fig. 3 **a** Schematic representation of the GAF constructs used for FRET experiments. Every 20-amino-acid sequence was regarded as a linker unit attached to the GAF domain. **b** Signal change in 2OG sensors. Δratio/R_{apo} for the eight FLIP sensors (relative to the original OGsor-G [*blue*]); OGsor-G-5 is not shown. Negative values indicate a decrease in the fluorescence intensity ratio (528 nm/478 nm) upon ligand addition; positive values indicate an increase in the ratio. **c** Ratio change for the eight FLIP sensors (relative to the original OGsor-G [*blue*]). **d** Normalized 2OG titration curves for OGsor-G-9 (*green*), OGsor-G-3 (*brown*), and OGsor-G-5 (*cyan*) in contrast with the original OGsor-G (*blue*) and OGsor-GA (*purple*). Data were analyzed in triplicate, and error bars indicate standard deviations

results for glucose, the addition of citrate had almost no effect on the intracellular 2OG level. Considering the complicated environment in the in vivo context, we also used *E. coli* cells expressing tandem fused YFP and CFP proteins as a negative control that showed no obvious ratio change upon the addition of carbon sources to exclude the possibility of a direct effect of the chromophores.

To determine whether environmental changes in 2OG concentrations affect the cellular steady-state levels of 2OG, we also monitored changes in 2OG levels in living *E. coli* cells after the addition of 2OG. The time-dependent decrease in the emission ratio following the addition of 10 mM 2OG is shown in Fig. 4c. Exogenous 2OG addition induced a decrease in the YFP/CFP emission ratio (i.e., an increase in the intracellular 2OG level), which indicates the transport of 2OG across the membrane. Addition of 2OG up to concentrations of 100 μM induced an increase in intracellular 2OG levels (Fig. 4f), which decreased the emission ratio. As shown in Fig. 4c, the intracellular 2OG levels in *E. coli* cells have a lag of approximately 5 min after the addition of 10 mM exogenous 2OG, which reflects the time required to activate and initiate the transport of extracellular 2OG. In contrast, glucose had an immediate marked effect on intracellular 2OG levels.

Changes in the intracellular 2OG level in response to the addition of glucose and 2OG were confirmed by measurement of 2OG pool concentrations with the HPLC method (Fig. 4d). The 2OG pool concentration decreased by 3-fold from 1.09 to 0.35 mM in *E. coli* cells moved from LB medium to M9 medium, and then increased by more than 6-fold from 0.35 to 2.63 mM or 2.14 mM at 30 min after addition of 10 mM glucose or 2OG to the M9 medium. These results are consistent with the FRET ratio data in Fig. 4b and c.

Table 2 Characterization of optimized biosensors

Sensor	AA	R_{apo}	R_{sat}	K_d	Δratio	Δratio/R_{apo} (%)
OGsor-G	0	1.38	1.22	687.4	−0.16	12
OGsor-G1	20	1.17	0.90	631.4	−0.27	23
OGsor-G2	40	1.24	0.88	579.1	−0.36	29
OGsor-G3	60	1.54	1.69	1923	0.15	10
OGsor-G4	80	1.04	0.77	564.9	−0.27	26
OGsor-G5	100	1.08	1.08	ND	0	0
OGsor-G6	120	1.04	0.75	473.2	−0.29	28
OGsor-G7	140	1.41	0.89	456.7	−0.52	37
OGsor-G8	160	1.48	0.86	381.0	−0.62	42
OGsor-G9	180	2.21	1.26	693.7	−0.95	43

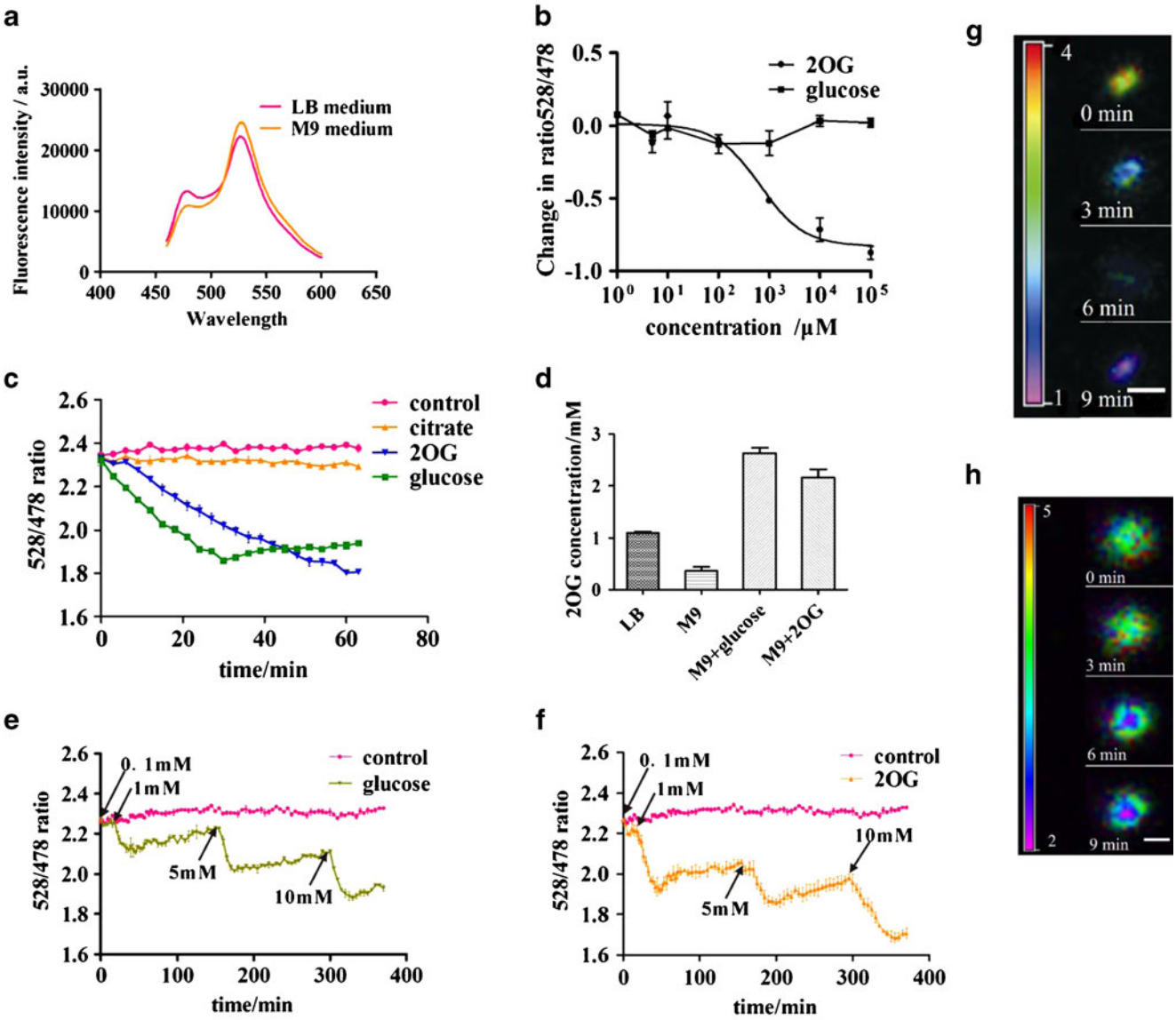

Fig. 4 **a** Comparison of BL21 (DE3)pLysS before (LB medium) and after starvation (M9 medium). **b** Comparison of glucose and 2OG addition at different concentrations of OGsor-G-9 in vitro as described previously. **c** Real-time monitoring of the nanosensor responding to different carbon sources (10 mM) in vivo. **d** 2OG pool measurements by HPLC under different conditions of 2OG metabolism. Real-time monitoring of the nanosensor responding to glucose (**e**) and 2OG (**f**) in vivo. The carbon source was added to the well in increasing concentrations. Data were analyzed in triplicate, and error bars indicate the standard deviation. Confocal fluorescence image obtained after addition of 2OG (**g**) and glucose (**h**), with the pseudocolor indicating a change in the YFP/CFP ratio after carbon source addition. Scale bar, 1 μm

To titrate the response to extracellular glucose and 2OG, cells expressing OGsor-G9 were further challenged with varying concentrations of glucose and 2OG (0.1, 1, 5, and 10 mM). Figure 4e and f shows the changes in the YFP/CFP emission ratio over time with increasing glucose and 2OG concentrations. The ratio was concentration dependent, which indicates that intracellular 2OG levels were correlated with glucose availability and extracellular 2OG concentration.

The ratio measurements were also obtained for single *E. coli* cells by using confocal microscopy. Glucose and 2OG were added to cells expressing OGsor-G9, and images were taken every 30 s for 9 min (Fig. 4g and h). The ratio images showed a time-dependent decrease in the fluorescence emission ratio in the cells, which was consistent with the results obtained using a microplate reader and demonstrates the feasibility of 2OG detection in *E. coli* at the level of a single living cell.

Discussion

Visualizing and monitoring cell activity in vivo with high spatial and temporal resolution is attractive because traditional analysis methods destroy living cells to extract metabolites of

interest. Since the discovery of GFP, scientists have used site-directed and random mutagenesis approaches to develop fluorescent protein mutants and have created a family of proteins that nearly span the complete fluorescence spectrum. These fluorescent proteins have been used to construct genetically encoded fluorescent biosensors for optical imaging of biochemical and physiological functions in living cells (Miranda et al. 2012; Salonikidis et al. 2011), and these indicators allow noninvasive spatiotemporal tracing of intracellular metabolism.

In the past decade, many fluorescent biosensors have been developed for monitoring key in vivo metabolites involved in carbon, nitrogen, and energy metabolism, including glucose, glutamine, glutamate, ATP, ADP, cAMP, and NADH (Depry et al. 2013). Recently, Ewald et al. described FRET-based sensors to detect citrate, which is an important intermediate in catabolic pathways involving glycolysis and the citric acid cycle (Ewald et al. 2011). Additionally, 2OG is also derived from the Krebs cycle, which is a highly conserved central metabolic pathway, and is at the interface between carbon and nitrogen metabolism. The central carbon intermediate 2OG serves as the sole carbon skeleton for the assimilation of nitrogen and participates in the generation of glutamate through the GS/GOGAT system. On the other hand, the conserved and ancient set of nitrogen sensor PII protein seems to respond to 2OG (as an allosteric effector), which is an indicator of the cellular nitrogen state. Thus, quantitatively tracing 2OG would be useful for studies on cell metabolism and signal transduction.

In the present study, to monitor intracellular 2OG levels, the 2OG-binding domain GAF of NifA protein was used to construct a genetically encoded FRET biosensor by attaching FP variants to each terminus of the GAF domain. Engineered sensors always require optimization to achieve better performance (Deuschle et al. 2005), such as site-directed mutagenesis of the binding pocket to generate mutants with binding affinities that overlap with physiological concentrations (Okumoto et al. 2005). Hires et al. (2008) performed systematic optimization of linkers to improve the sensitivity of the sensor by 6.2-fold. Our FRET-based sensors were optimized by insertion of peptide linkers with different lengths. The resulting sensor OGsor-G9 exhibited a maximal average ratio change ΔR of 0.95, which represented a 6-fold improvement over the ratio change of 0.16 observed for OGsor-G, and showed high selectivity for 2OG over other related compounds. The dynamic response range of OGsor-G9 is 100 μM to 10 mM and thus spans 2 orders of magnitude, which is consistent with the results for previously reported sensors (Fehr et al. 2002, 2003). Thus, this sensor covers a wide range of physiologically relevant 2OG concentrations.

We have demonstrated the value of this sensor by monitoring intracellular 2OG levels in living *E. coli* cells under various growth conditions. We found that 2OG accumulation caused by glucose addition was faster than that by direct 2OG addition. The reversible binding and dissociation between OGsor and 2OG was monitored in *E. coli* cells through addition and depletion of carbon sources in vivo, and we also obtained a sequential concentration-dependent signal with different concentrations of carbon sources. We have demonstrated that the rate of 2OG uptake mediated by the 2OG transporter KdgT (Partridge et al. 2006) and 2OG permease KgtP (Seol and Shatkin, 1991) is very high and that addition of 2OG itself has a significant effect on the intracellular 2OG level and metabolism (Fig. 4f). FRET ratio changes in single living *E. coli* cells responding to extracellular carbon were visualized using confocal microscopy. Our results illustrate that the OGsor is a powerful tool for evaluating the signal transduction and cross-talk mechanisms of central carbon metabolism and nitrogen metabolism in relation with the nutritional states of the cell.

As mentioned previously, 2OG stands at the crossroads between carbon and nitrogen metabolism, as important elements such as glutamate (Dulla et al. 2008; Hires et al. 2008) and glutamine (Gruenwald et al. 2012; Yang et al. 2010) from nitrogen metabolism and citrate (Ewald et al. 2011) from the Krebs cycle have already been exploited by genetically encoded fluorescent biosensors. It is therefore important to detect changes in 2OG levels to shed further light on carbon and nitrogen metabolism. 2OG also regulates many metabolic activities such as nitrogen metabolism (Teixeira et al. 2010), lipid absorption/metabolism, muscle performance, and cancerogenesis (Harrison and Pierzynowski 2008). Recent studies have also noted effects of 2OG on the condition of astroglia (Fomenko et al. 2011) and on gene expression in plant leaves (Araujo et al. 2012). With the attachment of a proper signal sequence, OGsor could be used to monitor 2OG in intracellular compartments of interest such as the plant cytosol (Bogner and Ludewig 2007), mitochondria, or nuclei and thus facilitate biological research.

Acknowledgments This study was supported by the China NSF (21276079), SRFDP (no. 20120074110009), the Key Grant Project (no. 313019) of the Chinese Ministry of Education, and the Fundamental Research Funds for the Central Universities.

References

Ansbacher T, Srivastava HK, Stein T, Baer R, Merkx M, Shurki A (2012) Calculation of transition dipole moment in fluorescent proteins—towards efficient energy transfer. Phys Chem Chem Phys 14(12):4109–4117. doi:10.1039/c2cp23351g

Araujo WL, Tohge T, Nunes-Nesi A, Daloso DM, Nimick M, Krahnert I, Bunik VI, Moorhead GB, Fernie AR (2012) Phosphonate analogs of 2-oxoglutarate perturb metabolism and gene expression in illuminated *Arabidopsis* leaves. Front Plant Sci 3:114. doi:10.3389/fpls.2012.00114

Aravind L, Ponting CP (1997) The GAF domain: an evolutionary link between diverse phototransducing proteins. Trends Biochem Sci 22(12):458–459. doi:10.1016/S0968-0004(97)01148-1

Bennett BD, Kimball EH, Gao M, Osterhout R, Van Dien SJ, Rabinowitz JD (2009) Absolute metabolite concentrations and implied enzyme active site occupancy in *Escherichia coli*. Nat Chem Biol 5(8):593–599. doi:10.1038/nchembio.186

Bogner M, Ludewig U (2007) Visualization of arginine influx into plant cells using a specific FRET-sensor. J Fluoresc 17(4):350–360. doi:10.1007/s10895-007-0192-2

Buck M, Gallegos MT, Studholme DJ, Guo Y, Gralla JD (2000) The bacterial enhancer-dependent sigma(54) (sigma(N)) transcription factor. J Bacteriol 182(15):4129–4136. doi:10.1128/JB.182.15.4129-4136.2000

Chen D, Duggan C, Ganley JP, Kooragayala LM, Reden TB, Texada DE, Langford MP (2004) Expression of enterovirus 70 capsid protein VP1 in *Escherichia coli*. Protein Expr Purif 37(2):426–433. doi:10.1016/j.pep.2004.06.027

Cicchetti G, Biernacki M, Farquharson J, Allen PG (2004) A ratiometric expressible FRET sensor for phosphoinositides displays a signal change in highly dynamic membrane structures in fibroblasts. Biochemistry 43(7):1939–1949. doi:10.1021/bi035480w

Depry C, Mehta S, Zhang J (2013) Multiplexed visualization of dynamic signaling networks using genetically encoded fluorescent protein-based biosensors. Pflugers Arch 465(3):373–381. doi:10.1007/s00424-012-1175-y

Deuschle K, Okumoto S, Fehr M, Looger LL, Kozhukh L, Frommer WB (2005) Construction and optimization of a family of genetically encoded metabolite sensors by semirational protein engineering. Protein Sci 14(9):2304–2314. doi:10.1110/ps.051508105

DiPilato LM, Cheng X, Zhang J (2004) Fluorescent indicators of cAMP and Epac activation reveal differential dynamics of cAMP signaling within discrete subcellular compartments. Proc Natl Acad Sci U S A 101(47):16513–16518. doi:10.1073/pnas.0405973101

Dulla C, Tani H, Okumoto S, Frommer WB, Reimer RJ, Huguenard JR (2008) Imaging of glutamate in brain slices using FRET sensors. J Neurosci Methods 168(2):306–319. doi:10.1016/j.jneumeth.2007.10.017

Ewald JC, Reich S, Baumann S, Frommer WB, Zamboni N (2011) Engineering genetically encoded nanosensors for real-time *in vivo* measurements of citrate concentrations. PLoS One 6(12):e28245. doi:10.1371/journal.pone.0028245

Fehr M, Frommer WB, Lalonde S (2002) Visualization of maltose uptake in living yeast cells by fluorescent nanosensors. Proc Natl Acad Sci U S A 99(15):9846–9851. doi:10.1073/pnas.142089199

Fehr M, Lalonde S, Lager I, Wolff MW, Frommer WB (2003) *In vivo* imaging of the dynamics of glucose uptake in the cytosol of COS-7 cells by fluorescent nanosensors. J Biol Chem 278(21):19127–19133. doi:10.1074/jbc.M301333200

Fehr M, Okumoto S, Deuschle K, Lager I, Looger LL, Persson J, Kozhukh L, Lalonde S, Frommer WB (2005) Development and use of fluorescent nanosensors for metabolite imaging in living cells. Biochem Soc Trans 33(Pt 1):287–290. doi:10.1042/BST0330287

Fomenko OZ, Ushakova HO, Piierzhynovs'kyi SH (2011) Astroglia proteins in the rat brain in experimental chronic hepatitis and 2-oxoglutarate effect. Ukr Biokhim Zh 83(1):69–76

Gruenwald K, Holland JT, Stromberg V, Ahmad A, Watcharakichkorn D, Okumoto S (2012) Visualization of glutamine transporter activities in living cells using genetically encoded glutamine sensors. PLoS One 7(6):e38591. doi:10.1371/journal.pone.0038591

Ha JS, Song JJ, Lee YM, Kim SJ, Sohn JH, Shin CS, Lee SG (2007) Design and application of highly responsive fluorescence resonance energy transfer biosensors for detection of sugar in living *Saccharomyces cerevisiae* cells. Appl Environ Microbiol 73(22):7408–7414. doi:10.1128/AEM.01080-07

Harrison AP, Pierzynowski SG (2008) Biological effects of 2-oxoglutarate with particular emphasis on the regulation of protein, mineral and lipid absorption/metabolism, muscle performance, kidney function, bone formation and cancerogenesis, all viewed from a healthy ageing perspective state of the art—review article. J Physiol Pharmacol 59(Suppl 1):91–106

Hires SA, Zhu Y, Tsien RY (2008) Optical measurement of synaptic glutamate spillover and reuptake by linker optimized glutamate-sensitive fluorescent reporters. Proc Natl Acad Sci U S A 105(11):4411–4416. doi:10.1073/pnas.0712008105

Ho YS, Burden LM, Hurley JH (2000) Structure of the GAF domain, a ubiquitous signaling motif and a new class of cyclic GMP receptor. EMBO J 19(20):5288–5299. doi:10.1093/emboj/19.20.5288

Honda A, Adams SR, Sawyer CL, Lev-Ram V, Tsien RY, Dostmann WR (2001) Spatiotemporal dynamics of guanosine 3′,5′-cyclic monophosphate revealed by a genetically encoded, fluorescent indicator. Proc Natl Acad Sci U S A 98(5):2437–2442. doi:10.1073/pnas.051631298

Imamura H, Nhat KP, Togawa H, Saito K, Iino R, Kato-Yamada Y, Nagai T, Noji H (2009) Visualization of ATP levels inside single living cells with fluorescence resonance energy transfer-based genetically encoded indicators. Proc Natl Acad Sci U S A 106(37):15651–15656. doi:10.1073/pnas.0904764106

Iqbal A, Arslan S, Okumus B, Wilson TJ, Giraud G, Norman DG, Ha T, Lilley DM (2008) Orientation dependence in fluorescent energy transfer between Cy3 and Cy5 terminally attached to double-stranded nucleic acids. Proc Natl Acad Sci U S A 105(32):11176–11181. doi:10.1073/pnas.0801707105

Jares-Erijman EA, Jovin TM (2006) Imaging molecular interactions in living cells by FRET microscopy. Curr Opin Chem Biol 10(5):409–416. doi:10.1016/j.cbpa.2006.08.021

John SA, Ottolia M, Weiss JN, Ribalet B (2008) Dynamic modulation of intracellular glucose imaged in single cells using a FRET-based glucose nanosensor. Pflugers Arch 456(2):307–322. doi:10.1007/s00424-007-0395-z

Kaper T, Lager I, Looger LL, Chermak D, Frommer WB (2008) Fluorescence resonance energy transfer sensors for quantitative monitoring of pentose and disaccharide accumulation in bacteria. Biotechnol Biofuels 1(1):11. doi:10.1186/1754-6834-1-11

Knetsch ML, Tsiavaliaris G, Zimmermann S, Ruhl U, Manstein DJ (2002) Expression vectors for studying cytoskeletal proteins in *Dictyostelium discoideum*. J Muscle Res Cell Motil 23(7–8):605–611

Lager I, Fehr M, Frommer WB, Lalonde S (2003) Development of a fluorescent nanosensor for ribose. FEBS Lett 553(1–2):85–89. doi:10.1016/S0014-5793(03)00976-1

Leigh JA, Dodsworth JA (2007) Nitrogen regulation in bacteria and archaea. Annu Rev Microbiol 61:349–377. doi:10.1146/annurev.micro.61.080706.093409

Martinez-Argudo I, Little R, Dixon R (2004) Role of the amino-terminal GAF domain of the NifA activator in controlling the response to the antiactivator protein NifL. Mol Microbiol 52(6):1731–1744. doi:10.1111/j.1365-2958.2004.04089.x

Martinez-Argudo I, Little R, Shearer N, Johnson P, Dixon R (2005) Nitrogen fixation: key genetic regulatory mechanisms. Biochem Soc Trans 33(Pt 1):152–156. doi:10.1042/BST0330152

Miranda JG, Weaver AL, Qin Y, Park JG, Stoddard CI, Lin MZ, Palmer AE (2012) New alternately colored FRET sensors for simultaneous monitoring of Zn(2)(+) in multiple cellular locations. PLoS One 7(11):e49371. doi:10.1371/journal.pone.0049371

Morett E, Segovia L (1993) The sigma 54 bacterial enhancer-binding protein family: mechanism of action and phylogenetic relationship of their functional domains. J Bacteriol 175(19):6067–6074

Nagai T, Yamada S, Tominaga T, Ichikawa M, Miyawaki A (2004) Expanded dynamic range of fluorescent indicators for Ca(2+) by circularly permuted yellow fluorescent proteins. Proc Natl Acad Sci U S A 101(29):10554–10559. doi:10.1073/pnas.0400417101

Nikolaev VO, Gambaryan S, Lohse MJ (2006) Fluorescent sensors for rapid monitoring of intracellular cGMP. Nat Methods 3(1):23–25. doi:10.1038/nmeth816

Okano H, Hwa T, Lenz P, Yan D (2010) Reversible adenylylation of glutamine synthetase is dynamically counterbalanced during steady-state growth of *Escherichia coli*. J Mol Biol 404:522–536. doi:10.1016/j.jmb.2010.09.046

Okumoto S, Looger LL, Micheva KD, Reimer RJ, Smith SJ, Frommer WB (2005) Detection of glutamate release from neurons by genetically encoded surface-displayed FRET nanosensors. Proc Natl Acad Sci U S A 102(24):8740–8745. doi:10.1073/pnas.0503274102

Partridge JD, Scott C, Tang Y, Poole RK, Green J (2006) *Escherichia coli* transcriptome dynamics during the transition from anaerobic to aerobic conditions. J Biol Chem 281(38):27806–27815. doi:10.1074/jbc.M603450200

Piston DW, Kremers GJ (2007) Fluorescent protein FRET: the good, the bad and the ugly. Trends Biochem Sci 32(9):407–414. doi:10.1016/j.tibs.2007.08.003

Ponsioen B, Zhao J, Riedl J, Zwartkruis F, van der Krogt G, Zaccolo M, Moolenaar WH, Bos JL, Jalink K (2004) Detecting cAMP-induced Epac activation by fluorescence resonance energy transfer: Epac as a novel cAMP indicator. EMBO Rep 5(12):1176–1180. doi:10.1038/sj.embor.7400290

Pos KM, Dimroth P, Bott M (1998) The *Escherichia coli* citrate carrier CitT: a member of a novel eubacterial transporter family related to the 2-oxoglutarate/malate translocator from spinach chloroplasts. J Bacteriol 180(16):4160–4165

Rajamani S, Zhu J, Pei D, Sayre R (2007) A LuxP-FRET-based reporter for the detection and quantification of AI-2 bacterial quorum-sensing signal compounds. Biochemistry 46(13):3990–3997. doi:10.1021/bi602479e

Salonikidis PS, Niebert M, Ullrich T, Bao G, Zeug A, Richter DW (2011) An ion-insensitive cAMP biosensor for long term quantitative ratiometric fluorescence resonance energy transfer (FRET) measurements under variable physiological conditions. J Biol Chem 286(26):23419–23431. doi:10.1074/jbc.M111.236869

Sato M, Ueda Y, Umezawa Y (2006) Imaging diacylglycerol dynamics at organelle membranes. Nat Methods 3(10):797–799. doi:10.1038/nmeth930

Senior PJ (1975) Regulation of nitrogen metabolism in *Escherichia coli* and *Klebsiella aerogenes*: studies with the continuous-culture technique. J Bacteriol 123(2):407–418

Seol W, Shatkin AJ (1991) *Escherichia coli* kgtP encodes an alpha-ketoglutarate transporter. Proc Natl Acad Sci U S A 88(9):3802–3806

Tanimura A, Morita T, Nezu A, Shitara A, Hashimoto N, Tojyo Y (2009) Use of fluorescence resonance energy transfer-based biosensors for the quantitative analysis of inositol 1,4,5-trisphosphate dynamics in calcium oscillations. J Biol Chem 284(13):8910–8917. doi:10.1074/jbc.M805865200

Teixeira PF, Selao TT, Henriksson V, Wang H, Noren A, Nordlund S (2010) Diazotrophic growth of *Rhodospirillum rubrum* with 2-oxoglutarate as sole carbon source affects regulation of nitrogen metabolism as well as the soluble proteome. Res Microbiol 161(8):651–659. doi:10.1016/j.resmic.2010.06.003

Yang H, Bogner M, Stierhof Y-D, Ludewig U (2010) H^+-independent glutamine transport in plant root tips. Transport 5

Yano T, Oku M, Akeyama N, Itoyama A, Yurimoto H, Kuge S, Fujiki Y, Sakai Y (2010) A novel fluorescent sensor protein for visualization of redox states in the cytoplasm and in peroxisomes. Mol Cell Biol 30(15):3758–3766. doi:10.1128/MCB.00121-10

Zhao MX, Jiang YL, He YX, Chen YF, Teng YB, Chen Y, Zhang CC, Zhou CZ (2010) Structural basis for the allosteric control of the global transcription factor NtcA by the nitrogen starvation signal 2-oxoglutarate. Proc Natl Acad Sci U S A 107(28):12487–12492. doi:10.1073/pnas.1001556107